Cardiovascular Pathology 26 (2016) 30–38

Contents lists available at ScienceDirect

Cardiovascular Pathology

Original Article

Peristrut microhemorrhages: a possible cause of in-stent neoatherosclerosis?

Zaven Terzian [a,b], T. Christian Gasser [c], Francis Blackwell [a,b], Fabien Hyafil [a,b], Liliane Louedec [a], Catherine Deschildre [a], Walid Ghodbane [b], Richard Dorent [a,b], Antonino Nicoletti [a], Marion Morvan [a], Mohammed Nejjari [a,d], Laurent Feldman [a,b], Graciela Pavon-Djavid [a,e], Jean-Baptiste Michel [a,*]

[a] INSERM U1148, Université Paris-Diderot, Sorbonne Paris-Cité, DHU-FIRE, Hôpital Bichat, Paris, France
[b] Departments of Cardiology, Nuclear Medicine, and Cardiac Surgery, Assistance Publique-Hôpitaux de Paris, DHU-FIRE, RHU iVASC, Hôpital Bichat, Paris, France
[c] Department of Solid Mechanics, School of Engineering Sciences, KTH Royal Institute of Technology, 100 44, Stockholm, Sweden
[d] Interventional Cardiology, Centre Cardiologique du Nord, Saint-Denis, France
[e] Paris13-Nord University-Villetaneuse, Villetaneuse, France

ARTICLE INFO

Article history:
Received 22 March 2016
Received in revised form 25 August 2016
Accepted 25 August 2016
Available online xxxx

Keywords:
Coronary artery disease
Stent
Neoatherosclerosis
Hemorrhage
Hemoglobin
Cholesterol

ABSTRACT

Background: In-stent neoatherosclerosis is characterized by the delayed appearance of markers of atheroma in the subintima, but the pathophysiology underlying this new disease entity remains unclear.
Methods and results: We collected 20 human coronary artery stents by removal from explanted hearts. The mean duration of stent implantation was 34 months. In all samples, neoatherosclerosis was detected, particularly in peristrut areas. It consisted of foam cells and cholesterol clefts, with or without calcification, associated with neovascularization. Iron and glycophorin-A were present in peristrut areas, as well as autofluorescent ceroids. Moreover, in response to neoatherosclerosis, tertiary lymphoid organs (tissue lymphoid clusters) often developed in the adventitia. Some of these features could be reproduced in an experimental carotid stenting model in rabbits fed a high-cholesterol diet. Foam cells were present in all samples, and peristrut red blood cells (RBCs) were also detected, as shown by iron deposits and *Bandeiraea simplicifiola* isolectin-B4 staining of RBC membranes. Finally, in silico models were used to evaluate the compliance mismatch between the rigid struts and the distensible arterial wall using finite element analysis. They show that stenting approximately doubles the local von Mises stress in the intimal layer.
Conclusions: We show here that stent implantation both in human and in rabbit arteries is characterized by local peristrut microhemorrhages and finally by both cholesterol accumulation and oxidation, triggering together in-stent neoatherosclerosis. Our data indicate that these processes are likely initiated by an increased mechanical stress due to the compliance mismatch between the rigid stent and the soft wall.

1. Introduction

Atherosclerotic lesions are major causes of death throughout the world [1]. The most vulnerable or unstable lesions are characterized by the presence of intraplaque hemorrhages [2]. Red blood cell (RBC) membranes represent an important source of nonesterified cholesterol and hemoglobin, a source of reactive iron, which catalyzes oxidation [2]. Coronary stents have been developed in order to increase the luminal diameter at the site of stenosis with the aim of relieving myocardial ischemia [3]. After stent implantation, intimal vascular smooth muscle cell (vSMC) hyperplasia takes place [4], leading to recurrent luminal narrowing (i.e., in-stent restenosis) [5]. To attempt to prevent this vSMC proliferation, bare-metal stents (BMSs) have been superseded by drug-eluting stents (DESs), coated with various antiproliferative drugs. Although the use of DESs has reduced the risk of in-stent restenosis, stent obstruction due to the development of in-stent neoatheroma and/or acute stent thrombosis [6] still remains an important clinical issue.

In-stent neoatherosclerosis may participate in complications after stent implantation, both by causing stenosis and by triggering thrombosis [7]. It corresponds to the delayed appearance, within the arterial tissue in close proximity to the stent struts, of lesions which share histopathologic characteristics with primitive atherosclerosis [8]. They appear more frequently (64% vs. 31%) and earlier (2 years after implantation, 29% vs. 0%) within DESs as compared to BMSs [7]. Karanasos et al., in a clinical study using optical coherence tomography (OCT),

Funding sources: This work was supported by the European Union under the Seventh Framework Program (FP7) PRESTIGE (PREvention of late Stent Thrombosis by an Interdisciplinary Global Effort), grant agreement number 260309.
Disclosures: none.
* Corresponding author at: INSERM U1148, Hôpital Xavier Bichat, 46 rue Henri Huchard, 75018, Paris, France. Tel.: +33 1 40 25 75 26; fax: +33 1 40 25 86 02.
E-mail address: jean-baptiste.michel@inserm.fr (J.-B. Michel).

http://dx.doi.org/10.1016/j.carpath.2016.08.007

suggested that neoatherosclerosis may also participate in late stent thrombosis [9]. To date, the pathophysiology underlying this new disease entity remains unclear. However, it is well established that intramural RBCs stimulate atherosclerosis via an accumulation of cholesterol-rich membranes and the promotion of local oxidative activities catalyzed by hemoglobin/iron release [2,10].

In order to explore the mechanism of intrastent neoatherosclerosis, we performed a detailed observation of human coronary stents obtained from explanted hearts in patients having undergone heart transplantation and used a stenting model in hypercholesterolemic rabbits to demonstrate the point. In addition, we used an in silico biomechanical approach to evaluate the compliance mismatch between the rigid struts and the distensible arterial wall during the cardiac cycle as the possible cause of peristrut microhemorrhages.

2. Methods

2.1. Human explanted hearts

Since 2010, 34 patients have received a heart transplant for ischemic heart disease in Xavier Bichat hospital in Paris. Among these patients, 10 had at least 1 coronary stent implanted before the transplantation and were included in the present analysis. The Institutional Review Board, IRB 0006477 of Hôpitaux Universitaires Paris-Nord Val de Seine, Paris 7 University, and Assistance Publique-Hôpitaux de Paris approved the use of explanted hearts for research. Following heart explantation, stented segments were removed, fixed in 4% PFA for 48 h, and then embedded in a methyl methacrylate resin. We collected 13 BMSs and 7 DESs (2 paclitaxel-, 2 zotarolimus-, and 2 everolimus-eluting stents and 1 unknown). Clinical data from transplanted patients are presented in Supplementary data and Supplementary Table 1.

2.2. Rabbit model of carotid atherosclerosis

Thirteen New Zealand white rabbits (mean weight, 3.5 kg; mean age, 4 months) were fed a 0.3% cholesterol-enriched diet as described [11]. After 15 days of high-fat diet, stents (6 BMSs and 7 DESs) were implanted in the right carotid artery using a right femoral access allowing the positioning of a 5-French introducer (Terumo, Tokyo, Japan) under general anesthesia. Stent characteristics are presented in Supplemental data. A 0.014-in. hydrophilic guidewire (Croos-it; Guidant, Indianapolis, IN, USA) permitted stent implantation (12 atm during 30 s). An intravenous bolus of 1000 IU of heparin sodium (Heparin Choay; Sanofi, Paris, France) was given immediately prior to stent implantation. Rabbits were sacrificed 4 weeks later by injection of a lethal dose (35 mg/kg) of sodium pentobarbital (Ceva Santé Animale, Paris, France), and the 13 stents were removed. The noninjured left carotid arteries were also collected and served as controls. This rabbit experimental design received approval from the Institutional Committee on Animal Research and Ethics (CARE, North Paris, no. 121, Paris 7 University) and was declared to the French Ministry of Research, no. 2012-15/698-0080.

2.3. Histological preparation

All arterial samples were embedded in methyl methacrylate (except controls, in paraffin) and cut into 12-μm-thick cross-sections using a dedicated microtome. Sections of stented arteries were depolymerized in a 2-methoxyethyl acetate solution and then stained.

Masson's trichrome staining was used for general histology and Alizarin red staining for calcification analysis. Perl's reaction was performed on all the samples, alone or amplified by 3,3′-diaminobenzidine (DAB) precipitation, to assess the presence of iron [12]. Alcian blue staining was used to identify glycosaminoglycans, with nuclear red counterstaining. vSMCs were detected with an anti-α-smooth muscle actin antibody in human (Abcam, Cambridge, UK) and in rabbit (Dako, Carpinteria, CA, USA) samples, revealed by DAB, with hematoxylin counterstaining. Phagocytes were identified with an anti-CD68 antibody in human samples (Dako, Carpinteria, CA, US) and the use of a DL649-conjugated secondary antibody (JIR 111496046; Johnson ImmunoResearch, West Grove, US). The RAM11 antibody was used to detect phagocytes in rabbit samples (Dako, Carpinteria, PA, USA), revealed by DAB, and counterstained with hematoxylin.

For the localization of RBC membranes in human samples, we used an anti-glycophorin A antibody (Abcam, Cambridge, UK), revealed by TRITC-conjugated secondary antibody (JIR 115026071; Johnson ImmunoResearch, West Grove, PA, USA). In rabbit samples, we used *Bandeiraea simplicifolia* isolectin-B4 (Sigma Chemicals, Perth, Australia), as previously described [13], with hematoxylin counterstaining. In order to detect ceroids, autofluorescence was observed at an emission wavelength of 605 nm [14] (see Table 1 for histological terms definitions).

To characterize the tertiary lymphoid organs (tissue lymphoid clusters), we performed immunostaining with anti-CD3 (pan-T antibody; Dako, Carpinteria, CA, USA) and anti-CD20 (B cell; Dako, Carpinteria, CA, USA) antibodies, which were respectively revealed by TRITC-conjugated (JIR 115026071; Johnson ImmunoResearch, West Grove, PA, USA) and DL649-conjugated (JIR 111496046; Johnson ImmunoResearch, West Grove, PA, USA) secondary antibodies. This classical histology was completed by a whole mount clearing technique, detailed in Supplemental data.

2.4. Biomechanics

In order to investigate stress concentration caused by coronary stenting, a finite element (FE) model was used [15] and detailed in Supplemental data.

2.5. Statistical analysis

Quantitative variables are expressed as means ± standard deviation and were compared using a Mann–Whitney nonparametric test. Qualitative variables are expressed as percentages and were compared with the Fischer's Exact Test. All *P* values are two-sided. A *P* value of .05 was considered significant. All analyses were performed using the MedCalc 14.10 software (MedCalc Software bvba, Ostend, Belgium).

3. Results

3.1. Coronary stents from human explanted hearts

Characteristics of patients and stents are shown in Supplementary Tables 1 and 2. The mean duration of stent implantation was 34±37 months (the range of stent implant duration was 0.3 to 96 months for BMSs and 0.3 to 70 months for DESs). BMSs were used only in patients (11/11) with acute coronary syndromes (ACSs), whereas the 7 DESs were used in patients with stable angina (4/7) or with ACSs (3/7).

Table 1
Definitions

	Definitions	Reference to figure
Foam cells	Fat-laden phagocytes (macrophages and/or smooth muscle cells) seen in atherosclerosis	1, 4, 5
Cholesterol cleft/crystal	Empty cleft present in deparafinized section corresponding to accumulation of cholesterol crystal (giving the geometrical aspect of the clefts)	1
Calcification	Localized accumulation of hydroxyapatite crystals	1
Neovessel	Acquired angiogenesis from adventitia toward media	5
Ceroids	Autofluorescent (550–605 nm) insoluble aggregates of lipids and proteins due to oxidation	3, 5
Tertiary lymphoid organs	Tissue lymphoid clusters in which adaptive immune maturation takes place, absent from media and usually present in the adventitia	2

Table 2
Histological characteristics

Human coronary stents	All stents (n=20)	BMS (n= 13)	DES (n=7)	
Peristrut foam cells, n (%)	20 (100)	13(100)	7 (100)	
Calcification, n (%)				
None	2 (10)	2 (15.5)	0 (0)	P=.52
+	3 (15)	3 (23)	0 (0)	P=.52
++	4 (20)	3 (23)	1 (14.3)	P=1.00
+++	11 (55)	5 (38.5)	6 (85.7)	P=.07
Adventitial accumulation of lymphocytes, n (%)	10 (50)	5 (38.5)	5 (71.4)	P=.35
Cholesterol crystals, n (%)	7 (35)	3 (23)	4 (57.1)	P=.17
Positive Perl's reaction, n (%)	18 (90)	12 (92.3)	6 (85.7)	P=1.00
Positive Perl's + DAB reaction, n (%)	20 (100)	13 (100)	7 (100)	
Hemoglobin autofluorescence, n (%)	20 (100)	13 (100)	7(100)	
Ceroids, n (%)	5 (25)	5 (38)	0 (0)	P=.11
Stent thrombosis, n (%)	4 (20)	3 (23)	1 (14.4)	P=1.00
Rabbit carotid stents	**All stents (n= 13)**	**BMS (n=6)**	**DES (n=7)**	
Peristrut foam cells, n	13	6	7	
Positive Perl's reaction, n	4	3	1	P=.26
Positive Perl's + DAB reaction, n	13	6	7	
RBC membranes in subintima,[a] n	13	6	7	
Presence of phagocytes,[b] n	13	6	7	
Ceroids, n (%)	2 (15.4)	2 (33)	0 (0)	P=.19

[a] Isolectin-B4 staining.
[b] RAM-11.

Neoatherosclerotic lesions were present in all coronary stents (Table 2), characterized by the presence of foam cells, particularly in peristrut areas, and the presence of cholesterol crystal clefts, associated with foci of calcification, alcianophilic fibrocellular intimal proliferation, medial neoangiogenesis, and adventitial tissue lymphoid clusters (Figs. 1 and 2). The neoangiogenesis originating from the adventitia was sometimes very intense, and RBCs were frequently observed in close contact of stent struts (Fig. 1A and B). As compared to primary coronary atheroma, these lesions

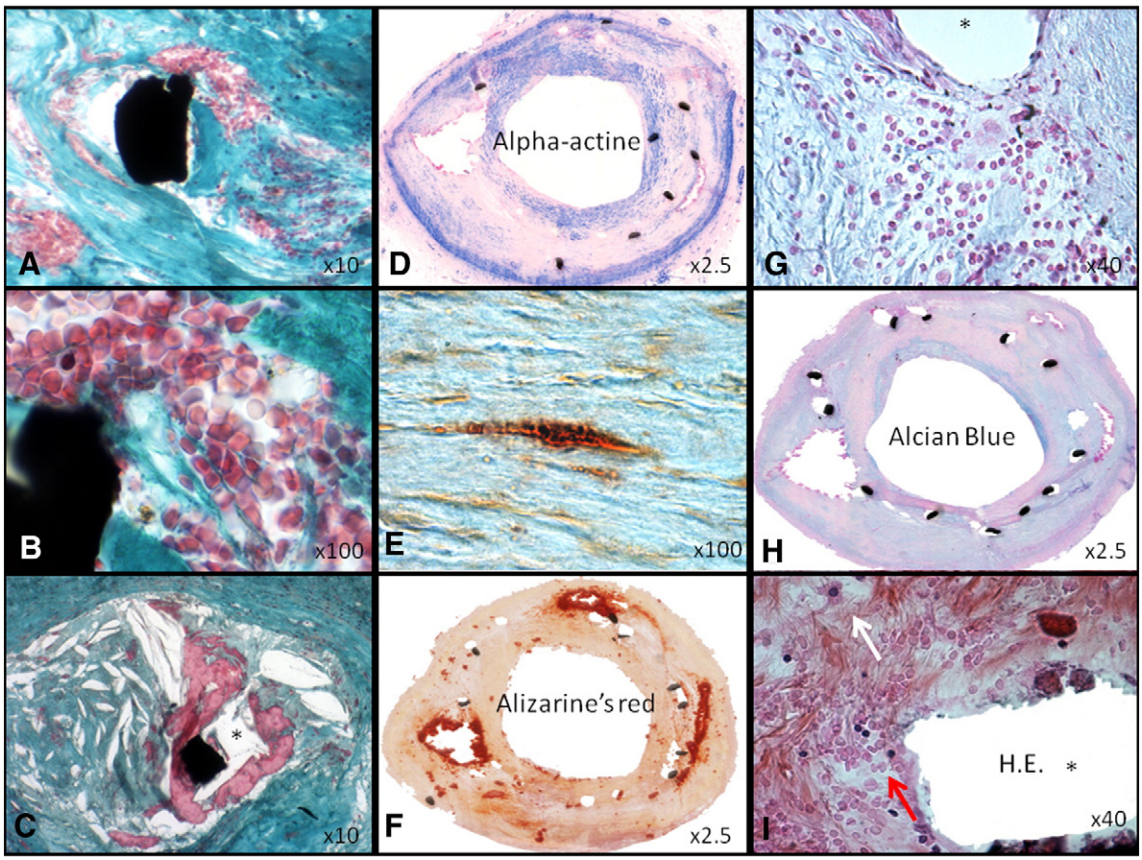

Fig. 1. Histology of neoatherosclerosis in a coronary bare metal stent. The BMS was implanted 96 months before heart transplantation in the circumflex artery of a 58-year-old patient with a history of ACSs. (A–C) Masson's trichrome. (A and B) The stent strut (black) is surrounded by presence of intact RBCs (B, ×100). (C) Empty clefts corresponding to extracellular solid crystals of cholesterol accumulation associated with free hemoglobin in red. (D) α-actin staining in blue. (E and F) Alizarin red staining of hydroxyapatite. (G and H) Alcian blue staining of proteoglycans. (I) Hematoxylin/eosin staining showing RBCs (red arrow) without nuclei and foam cells (white arrow) in the peristrut area.

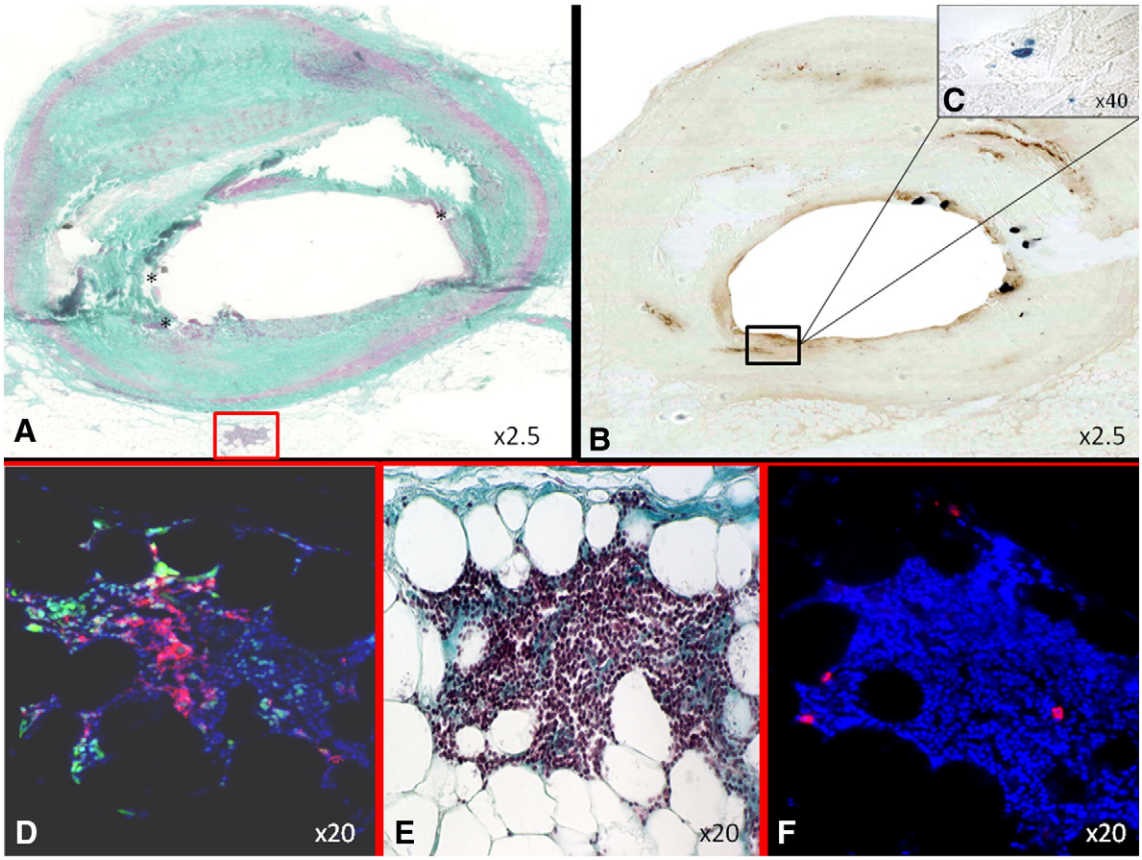

Fig. 2. Immune response to in-stent neoatherosclerosis in a paclitaxel-eluting stent. The DES was implanted 285 days before heart transplantation in the proximal section of the left anterior descending artery in a 52-year-old patient with a history of ACSs. (A) Masson's trichrome: note the leukocytes clusters (red box area) in the adventitial layer surrounded by adipocytes (E). In the intima, asterisks represent stent struts. (B) Perl's + DAB reaction of the same sample showed iron deposits near the stent strut. (C) High magnification showed, after Perl's reaction, the presence of iron (blue) in foam cells. (D) CD-3 (green) and CD-20 (red) staining. CD-3 lymphocytes (T cells) are located in the periphery of the cluster, whereas CD-20 lymphocytes (B cells) are in the center. (F) CD68 (red) staining showing the rare presence of phagocytes in the cluster.

were situated more deeply in the wall and were covered by a thicker fibrocellular cap, always in relation with peristrut areas at the intima/media interface.

Peristrut microhemorrhages were found in all cases (Table 2 and Fig. 3), as detected directly by the presence of intact RBCs (Fig. 1A and B) or the presence of modified extracellular hemoglobin associated with crystal clefts (Fig. 1C), or indirectly by the accumulation of reactive iron by Perl's reaction and/or Perl's reaction followed by DAB precipitation (Fig. 3F–I), red autofluorescent ceroids (Fig. 3D), and glycophorin A immunodetection (Fig. 3E). Due to their different metabolic pathways and the varied times of sampling with respect to the evolution of the pathology, these markers were not always colocalized. Cholesterol crystal clefts were sometimes colocalized with these markers. Peristrut foam cells were predominantly Perl's + DAB positive, providing evidence of iron accumulation within phagocyte vacuoles. These phagocytes were frequently α-smooth muscle actin positive.

Calcifications were very frequent (18/20) and mainly developed as nuclei (Fig. 1F) but were also observed as small focalized deposits, sometimes in a single vSMC (Fig. 1E).

In 50% of the sections (Table 2), lymphocyte clusters, containing B cells, were detected in the adventitia of the stented coronary artery (Fig. 2), indicating that an immune response was undergoing maturation within the adventitial layer.

Due to the small number of samples and to the heterogeneity of stenting duration, it was not possible to establish any histological differences between DESs and BMSs.

3.2. Rabbit samples

Histological characteristics are detailed in Table 2. Atheromatous lesions (Fig. 4) in contralateral carotid arteries (controls) were exclusively composed of focal subendothelial foam cells, protruding into the lumen (Fig. 4I and L). In contrast, in-stent neoatherosclerosis was associated with subintimal peristrut foam cell clusters, observed in all samples (Fig. 4C), and these cells were identified as vSMCs after α-smooth muscle actin staining (Fig. 4G and H) and associated with Alcian blue (Fig. 4J and K) staining. RAM 11+ phagocytes were detected in the intima (Fig. 4F). As in humans, neoangiogenesis was observed, and the presence of RBCs could be also detected in the peristrut area (Fig. 5E and F).

Control lesions were negative for iron detection (not shown). In contrast, peristrut RBCs were present in stented sections (Fig. 5) and were characterized by the presence of iron (Perl's and Perl's + DAB reaction), of isolectin-B4-positive RBC membranes in the subintima near the stent struts, and of ceroids. Isolectin-B4 also identified neovessels and punctual microhemorrhage in close contact of struts (Fig. 5E and F). Contrasting with Perl's + DAB positivity, which predominated in peristrut areas, positive isolectin-B4 staining was not limited to these peristrut areas but also extended to the intima in close relation to the lumen, independently of the struts (Fig. 5D). We found that the foam cells were able to engulf RBCs present in their vicinity (Fig. 5G). Autofluorescent ceroids were detected in only two BMS samples. In all the samples, a red autofluorescence was present directly on the metal of the stent struts, suggesting the presence of hemoglobin not only in the peristrut area but also at the interface with the metal (Fig. 5I).

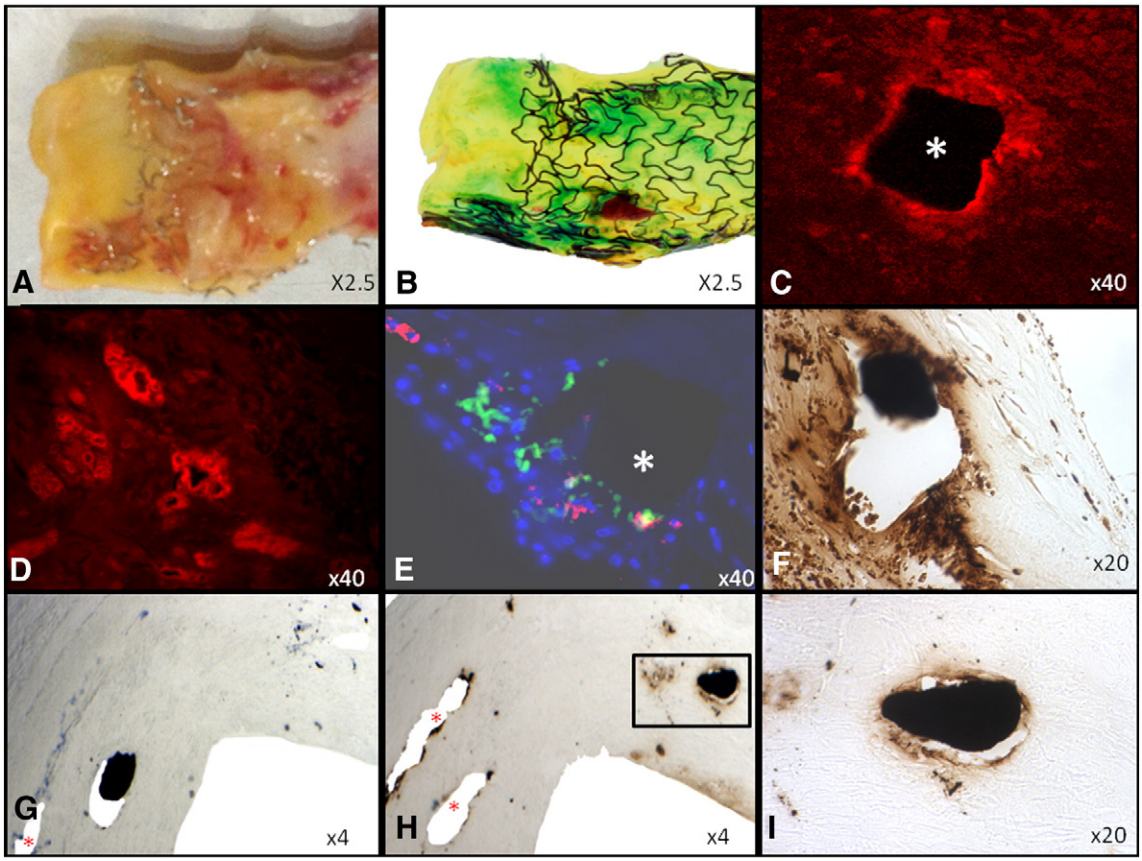

Fig. 3. Peristrut hemorrhages after human coronary stenting. (A and B) Paclitaxel-eluting stent implanted 66 months before heart transplantation in the right coronary artery of a 52-year-old patient. (A) Macroscopic view of the stent after longitudinal section. The stent is covered by a neointima, and bleeding in the arterial wall is visible in red. (B) The same stent after clarification (whole mount technique) using Perl's staining (green) and Alizarin red (calcium), suggesting iron deposits close to the stent struts. (C and D) BMS implanted in the right coronary artery 15 days before transplantation in a 64-year-old patient. Autofluorescence at 605-nm wavelength revealing red staining on the stent strut (white asterisk) and the presence of ceroid rings (D). (E) Immunohistochemistry using anti-glycophorin-A (green) and anti-CD68 (red) antibodies (BMS implanted 10 days before heart transplantation in a 65-year-old patient). The white asterisk localizes the stent strut. (F) Perl's + DAB reaction (paclitaxel-eluting stent implanted 70 months before transplantation in the circumflex artery of a 56-year-old patient). (G–I) Perl's (G) and Perl's + DAB reaction (H and I) of a BMS implanted 96 months before heart transplantation in the circumflex artery of a 58-year-old patient. Red asterisks correspond to stent struts location.

3.3. Biomechanical stress induced by solid strut/soft arterial wall interactions (Fig. 6)

The von Mises stress plot from our FE analysis is shown in Fig. 6b. This plot nicely illustrates that stenting approximately doubles the local von Mises stress in the intimal layer, i.e., from about 70 kPa that is seen in the intimal sections away from the stent strut to peaks of 150 kPa directly underneath the stent strut. Naturally, the normal stress in the radial vessel direction (radial normal stress), i.e., along which the strut pushes, is massively influenced. Specifically, in our simulation, stenting elevated the magnitude of the local radial stress from 13.3 kPa (100 mmHg) to about 200 kPa (Fig. 6c). Finally, the inhomogeneous loading by stent struts causes local shear stress in the radial–longitudinal plane and close to the strut (Fig. 6d). The magnitude of this shear stress increases from zero kPa (solution of the inflated axisymmetric vessel) to peaks at 55 kPa.

4. Discussion

In our studies of stent pathology, we consistently found in-stent neoatherosclerosis, both in a series of human coronary stents obtained from explanted hearts before heart transplantation and in an experimental model of carotid stenting in the hypercholesterolemic rabbit. Several mechanisms have been suggested [16] like foreign body chronic inflammation as a response to the stent, aberrant endothelial cell function, and incomplete cell coverage. Neoatherosclerotic lesions are located predominantly in the deeper layers of the subintima, around the stent struts, rebutting an endothelial dysfunction ore a defect in cell coverage. This observation, together with the results of our finite element study, strongly suggests that the biomechanical interaction between the rigid stent struts and the surrounding soft tissue may play a causal role in neoatherosclerosis formation. In addition, both in humans and in the rabbit model, we found RBCs and oxidative iron in the vicinity of the stent struts, which may be a consequence of the friction at the stent strut/vessel wall interface during the cardiac cycle. Finally, neoatherosclerosis was often associated with an immune adaptative response in the adventitia. Our results are in line with the findings of Nakazawa et al. [7], who studied a large autopsy cohort of stents; described lesion morphologies, including plaque rupture, fibroatheroma, calcifications, and pathological intimal thickening; and finally compared BMSs and DESs. However, our observations significantly extend the latter study, providing additional information on peristrut microhemorrhages.

4.1. Peristrut hemorrhages

Because of their rigidity, stents cannot fully accompany the pulsatility (extension and retraction) of epicardial coronary vessels during the cyclic stretches imposed by systolodiastolic motion. The interface between the solid metallic material of the stent and the soft viscoelastic arterial wall is therefore subjected to very specific stresses. Such biomechanical mismatch has been studied in the context of arterial wall calcifications associated with atherosclerosis [17,18] but not in relation to the arterial wall reaction to stent implantation. In this context, rigid inclusions (calcifications or struts)

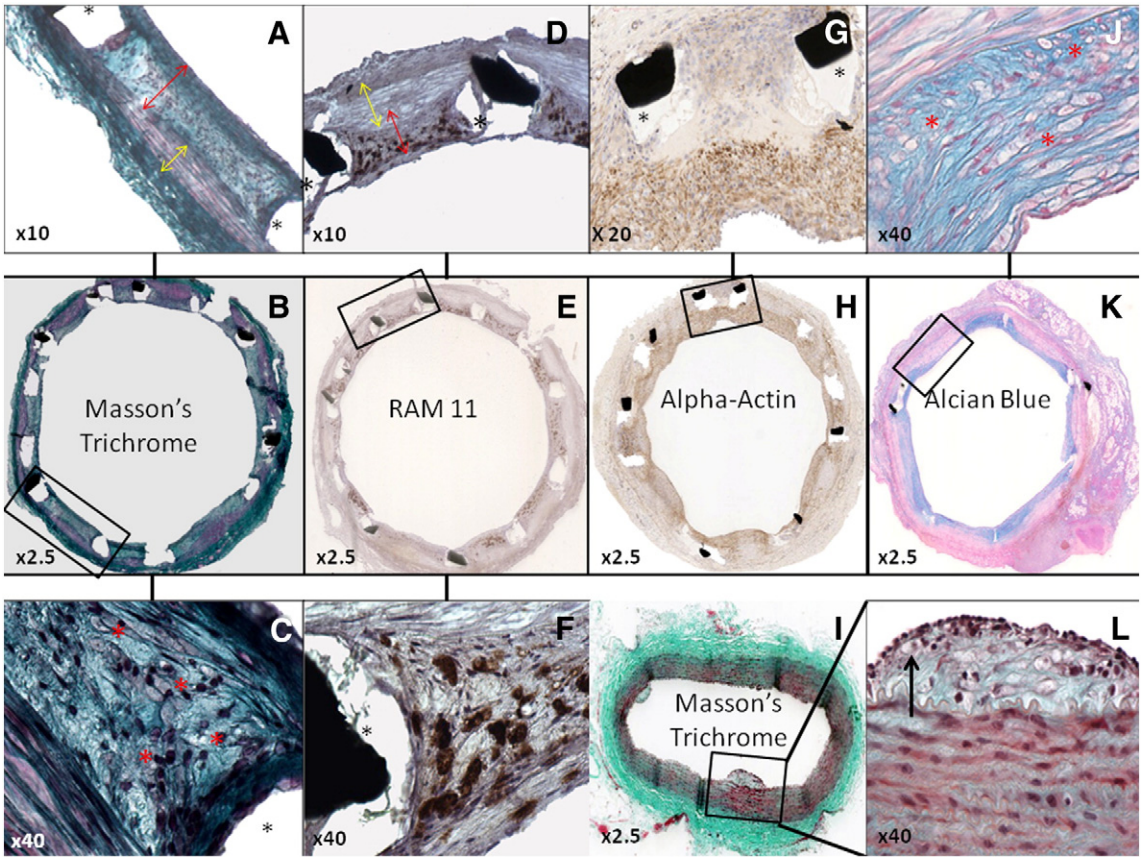

Fig. 4. Histology of in-stent neoatheroma in rabbit carotid arteries after implantation of a BMS. (A–C) Masson's trichrome. The media is represented by the yellow arrow; the neointima, by the red arrow. The asterisk denotes the stent strut location. At high magnification of the boxed area in B, foam cells are visible in the subintima (red asterisks), corresponding to neoatherosclerotic lesions, close to the stent strut. (D–F) RAM 11 staining. RAM 11 appears brown in the subintima (red arrow) between two stent struts (asterisks). There is no RAM 11 staining in the media (yellow arrow). The high magnification of the boxed area shows RAM 11 staining of the foam cells (phagocytes) located close to the stent strut (asterisk). (G and H) α-actin staining appearing in brown in the neointima and in the media. (I and L) Controls (nonstented left carotid artery). Foam cell (black arrow) accumulation is present in the subendothelial layer; budding (boxed area), in the arterial lumen). (J and K) Alcian blue. Blue staining appears in the media and subintima. Background of foam cells is positive for glycosaminoglycan staining.

in the distensible arterial wall can introduce mismatch and failure stress with tears at the interface between compliant (soft tissue) and noncompliant (struts) components. We found that calcifications, which are also hard tissues, cause "pericalcification hemorrhages" in the surrounding tissue with iron deposits detected by Perl's and Perl's + DAB reaction (Fig. 3). This observation confirms the presence of a physical frontier between hard and soft tissues, which has consequences for the biology of the tissue in the vicinity of this interface. Similarly to pericalcification hemorrhages [19], stenting not only severely elevates local stress levels but also introduces a completely nonphysiological stress pattern. Due to the pulsatile loading of the vasculature, such stress may lead to fatigue-like microdamage, i.e., microscopic tears of the soft tissue surrounding the stent as observed in the present study. Most importantly, the layered structure of the vessel wall may be vulnerable either to the nonphysiological shear stress in the radial longitudinal plane (Fig. 6d) or to the high von Mises stress induced by stenting, which in turn may trigger microscopic tears. This compliant mismatch leading to intratissular microhemorrhages could explain the accelerated nature of in-stent neoatherosclerosis as compared to atherosclerosis arising in native arteries.

4.2. From peristrut microhemorrhages to in-stent neoatherosclerosis

Whereas intraplaque hemorrhages are involved in the progression of atherosclerotic lesions [20], leading to their vulnerability and rupture [2], peristrut microhemorrhages with accumulation of RBCs appear to be at the origin of in-stent neoatherosclerotic lesions. RBCs lose their cellular structure and release membranous lipids and hemoglobin. RBC membranes are particularly rich in free and unesterified cholesterol [21] and are hence a source of cholesterol crystal formation in intraplaque hemorrhage [10,22].

Hemoglobin, composed of globin and iron-rich heme, is phagocytosed, forming foam cells [23], and undergoes proteolysis, producing globin degradation products and free heme. In physiologic conditions, heminic iron is in the ionized ferrous form (Fe^{2+}, oxyhemoglobin) [24]. Fe^{3+} heme (ferric methemoglobin) dissociates more easily from globin than Fe^{2+}, releasing deleterious hydrophobic free heme/iron [25]. Heme is metabolized by HO-1 to produce free iron, CO, and biliverdin [2]. Ionized iron can mediate oxidative modifications of lipids, proteins, and DNA and cause cytotoxicity [26,27], and therefore amplifies the oxidation capacity (Fenton and Haber–Weiss reactions) of biological systems [28]. Iron retention can be visualized by Prussian blue (Perl's) reaction. The use of Perl's + DAB reaction was required to increase sensitivity [12]. It is now well established that the presence of RBCs within the arterial wall in humans [10] as well as in rabbits [29] enhances the development of atherosclerosis. Our histologic results are also in line with previous OCT findings [30].

4.3. Adventitial adaptive immune response to in-stent neoatherosclerosis

After arterial injury, remodeling involves the entire wall. The adventitia is the outermost layer of the arterial wall, in which the adaptive immune response takes place [31]. In our study, we noted an adaptive immune reaction resulting in tertiary lymphoid organs (tissue lymphoid clusters) formation not only with T cells but also with the

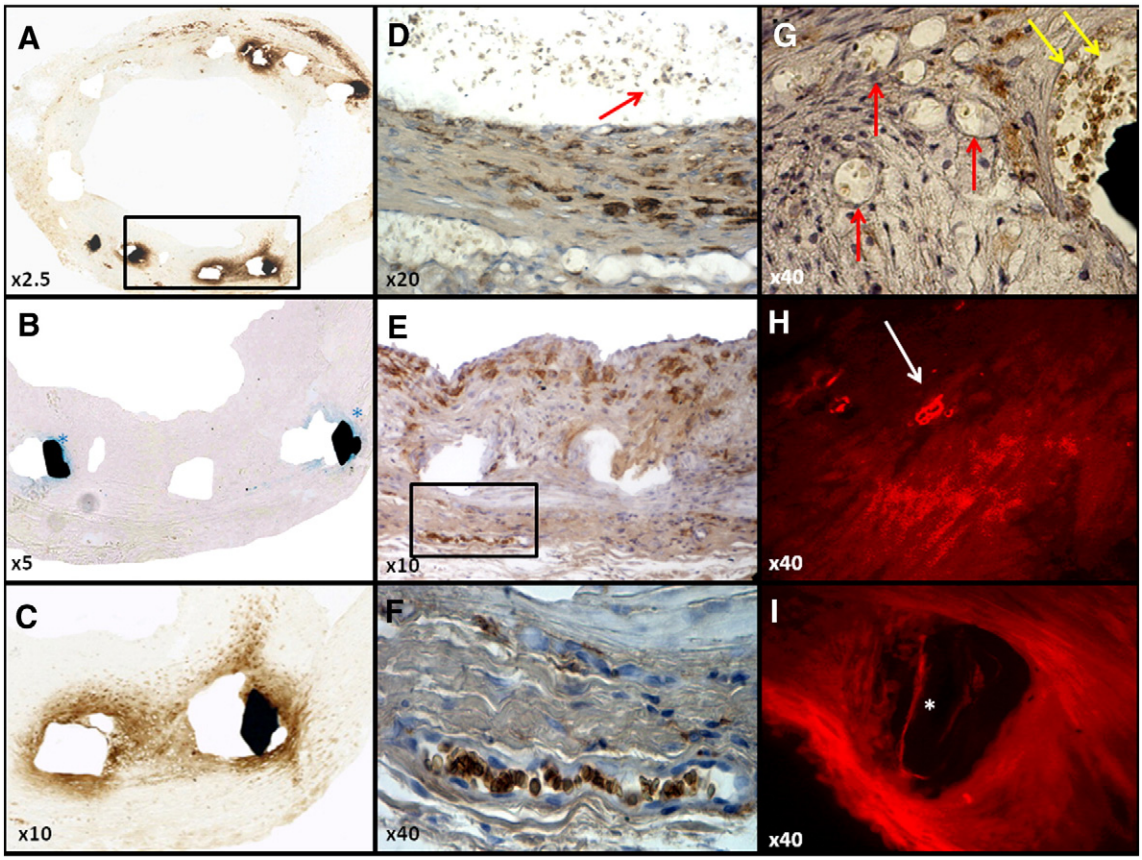

Fig. 5. Histology of peristrut hemorrhages in rabbit stenting. (A–C) Iron presence. (A) General view of Perl's + DAB reaction showing a large quantity of iron (brown staining) in the peristrut (asterisks) areas. (B)– High magnification of the black boxed area in A suggesting that iron is preferentially located in peristrut areas. (C) Iron is visualized by Perl's staining (blue asterisks) in the same areas as in B. (D–G) Isolectin B4 staining (IB4). (D) Intact RBCs are located in the lumen (red arrow), and IB4 staining is positive in the intima (brown). (E and F) A vascular structure is located close to the stent strut location (white), with intact RBCs (F). (G) IB4 staining is positive in peristrut areas (yellow arrow) and in foam cells (red arrows), suggesting that RBCs have been phagocytosed by foam cells. (H and I) Ceroids are visible at a wavelength of 605 nm and show a red autofluorescence (H, white arrow). Note the red autofluorescence of the stent strut (white asterisk), also at 605-nm wavelength (I).

presence of B cells and phagocyte markers (Fig. 2), probably in response to in-stent RBCs and oxidation-rich neoatherosclerosis. These lymphocyte tissue clusters are reminiscent of tertiary lymphoid organs described in chronic rejection [32], atherosclerosis [33], and aortic aneurysms [34]. These results suggest a relationship between intramural RBC release, tissue oxidation, and the development of an adaptive immune response within the adventitia.

4.4. Clinical relevance

Peristrut RBC release, the adventitial immune response, and in-stent neoatherosclerosis may all participate in the formation of an "in-stent vulnerable plaque" phenotype which has been described in postmortem studies of late and very late stent thrombosis [35,36].

4.5. Limits

First, neither our human nor our experimental studies were sufficiently powered to detect a qualitative or quantitative difference between the neoatherosclerotic lesions of BMSs versus DESs. The profile of patients in our study (severe ischemic cardiomyopathy treated by heart transplantation) and the limited number of cases could explain the high frequency of in-stent neoatherosclerosis and the absence of difference between DESs and BMSs. Second, in the experimental rabbit model, the delay between stent implantation and sampling was relatively short (4 weeks), probably explaining why cholesterol crystals, calcifications, or tissue lymphoid clusters were not observed. But it allowed us to confirm the presence and putative role of peristrut RBC release in the formation of iron-rich foam cells. Third, methacrylate embedding limits the use of immunohistochemistry. This point probably explains why we did not succeed in immunostaining microvessels by CD31 antibodies even in the adventitia.

5. Conclusion

This observational and experimental study, despite the relatively limited number of samples analyzed, highlights peristrut microhemorrhages and RBC accumulation and metabolism as a possible cause of the formation of in-stent neoatherosclerotic lesions. Our data strongly suggest that these lesions are induced by the physical shear between the metallic strut and the soft arterial wall, which display specific stress features during systole/diastolic motion.

Acknowledgments

Zaven Terzian, Francis Blackwell, and Mohammed Nejjari were supported by the Fédération Française de Cardiologie. The authors want to thank the INSERM U1148 biobank and the histopathology department of Hôpital Bichat for material support and Mary Osborne Pellegrin for the English editing.

Appendix A. Supplementary data

Supplementary data to this article can be found online at http://dx.doi.org/10.1016/j.carpath.2016.08.007.

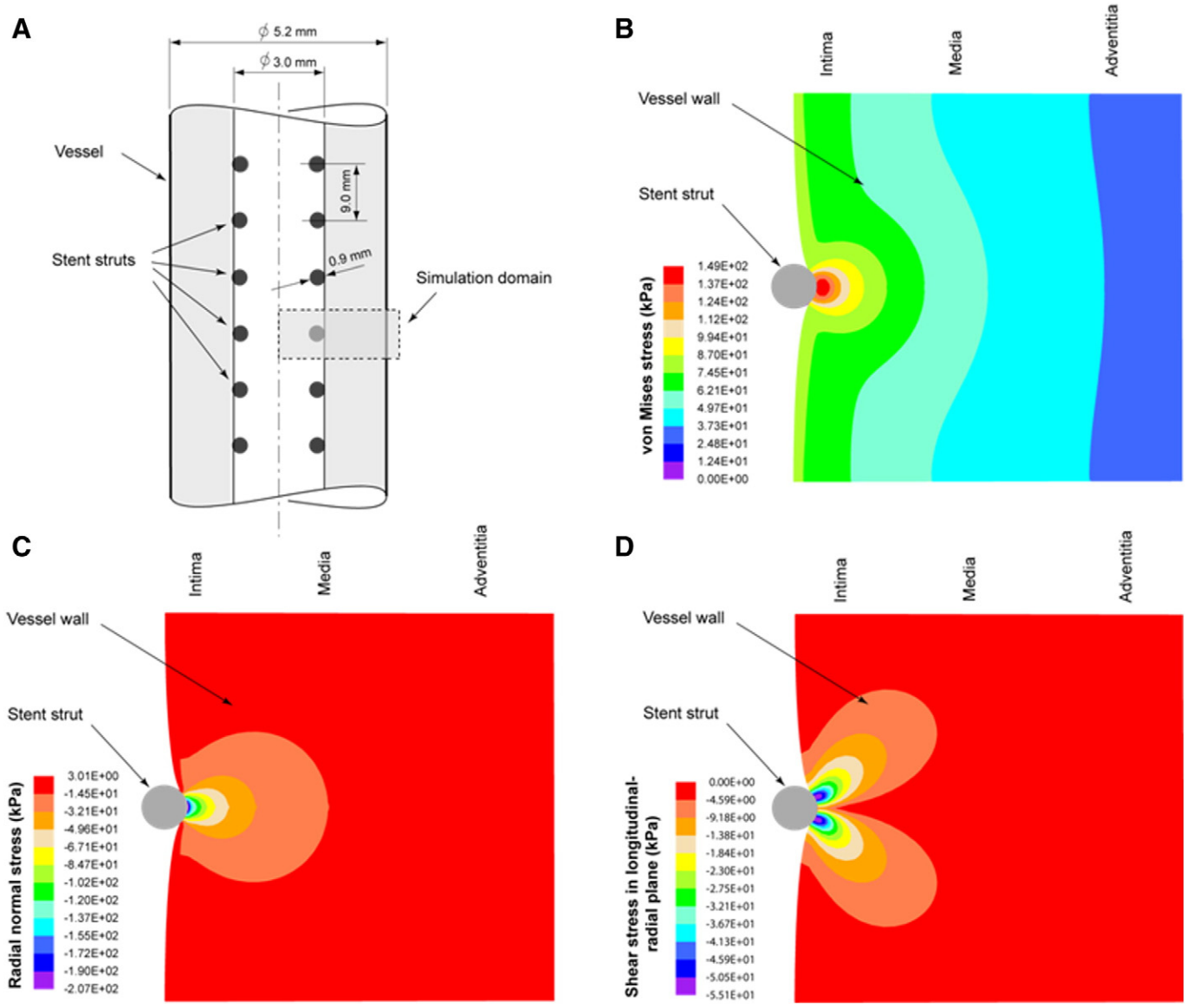

Fig. 6. Stress analysis of a stented coronary artery: (A) idealized model with dimensions. The vessel segment denoted by "Simulation domain" was modeled with the FE method in order to investigate wall stress underneath the stent strut. (B) von Mises stress distribution in the coronary vessel wall illustrating that stenting doubles the local stress level in the intimal layer. (C) Normal stress in the radial vessel direction reaches a compression of 200 kPa underneath the stent strut. (D) Inhomogeneous loading by the stent struts causes local shear stress magnitudes of 55 kPa in the longitudinal–radial plane of the vessel wall.

References

[1] Roger VL, Go AS, Lloyd-Jones DM, Adams RJ, Berry JD, Brown TM, et al. Heart disease and stroke statistics—2011 update: a report from the American Heart Association. Circulation 2011;123:e18-209. http://dx.doi.org/10.1161/CIR.0b013e3182009701.

[2] Michel J-B, Virmani R, Arbustini E, Pasterkamp G. Intraplaque haemorrhages as the trigger of plaque vulnerability. Eur Heart J 2011;32:1977–85. http://dx.doi.org/10.1093/eurheartj/ehr054.

[3] Keeley EC, Boura JA, Grines CL. Primary angioplasty versus intravenous thrombolytic therapy for acute myocardial infarction: a quantitative review of 23 randomised trials. Lancet 2003;361:13–20. http://dx.doi.org/10.1016/S0140-6736(03)12113-7.

[4] Welt FGP, Rogers C. Inflammation and restenosis in the stent era. Arterioscler Thromb Vasc Biol 2002;22:1769–76. http://dx.doi.org/10.1161/01.ATV.0000037100.44766.5B.

[5] Austin GE, Ratliff NB, Hollman J, Tabei S, Phillips DF. Intimal proliferation of smooth muscle cells as an explanation for recurrent coronary artery stenosis after percutaneous transluminal coronary angioplasty. J Am Coll Cardiol 1985;6:369–75. http://dx.doi.org/10.1016/S0735-1097(85)80174-1.

[6] Palmerini T, Biondi-Zoccai G, Della Riva D, Stettler C, Sangiorgi D, D'Ascenzo F, et al. Stent thrombosis with drug-eluting and bare-metal stents: evidence from a comprehensive network meta-analysis. Lancet 2012;379:1393–402. http://dx.doi.org/10.1016/S0140-6736(12)60324-9.

[7] Nakazawa G, Otsuka F, Nakano M, Vorpahl M, Yazdani SK, Ladich E, et al. The pathology of neoatherosclerosis in human coronary implants bare-metal and drug-eluting stents. J Am Coll Cardiol 2011;57:1314–22. http://dx.doi.org/10.1016/j.jacc.2011.01.011.

[8] Inoue T, Shinke T, Otake H, Nakagawa M, Hariki H, Osue T, et al. Neoatherosclerosis and mural thrombus detection after sirolimus-eluting stent implantation. Circ J 2014;78:92–100. http://dx.doi.org/10.1253/circj.CJ-13-0374.

[9] Karanasos A, Ligthart JMR, Regar E. In-stent neoatherosclerosis: a cause of late stent thrombosis in a patient with "full metal jacket" 15 years after implantation: insights from optical coherence tomography. JACC Cardiovasc Interv 2012;5:799–800. http://dx.doi.org/10.1016/j.jcin.2012.02.020.

[10] Kolodgie FD, Gold HK, Burke AP, Fowler DR, Kruth HS, Weber DK, et al. Intraplaque hemorrhage and progression of coronary atheroma. N Engl J Med 2003;349:2316–25. http://dx.doi.org/10.1056/NEJMoa035655.

[11] Rosenfeld ME, Ross R. Macrophage and smooth muscle cell proliferation in atherosclerotic lesions of WHHL and comparably hypercholesterolemic fat-fed rabbits. Arteriosclerosis 1990;10:680–7. http://dx.doi.org/10.1161/01.ATV.10.5.680.

[12] Meguro R, Asano Y, Odagiri S, Li C, Iwatsuki H, Shoumura K. Nonheme-iron histochemistry for light and electron microscopy: a historical, theoretical and technical review. Arch Histol Cytol 2007;70:1–19. http://dx.doi.org/10.1679/aohc.70.1.

[13] Tziakas D, Chalikias G, Kapelouzou A, Tentes I, Schäfer K, Karayannakos P, et al. Erythrocyte membrane cholesterol and lipid core growth in a rabbit model of atherosclerosis: modulatory effects of rosuvastatin. Int J Cardiol 2013;170:173–81. http://dx.doi.org/10.1016/j.ijcard.2013.10.070.

[14] Haka AS, Kramer JR, Dasari RR, Fitzmaurice M. Mechanism of ceroid formation in atherosclerotic plaque: in situ studies using a combination of Raman and fluorescence spectroscopy. J Biomed Opt 2011;16:11011. http://dx.doi.org/10.1117/1.3524304.
[15] Wriggers P. Computational contact mechanics. 1st ed. Hoboken, USA: Wiley; 2002.
[16] Komiyama H, Takano M, Hata N, Seino Y, Shimizu W, Mizuno K. Neoatherosclerosis: coronary stents seal atherosclerotic lesions but result in making a new problem of atherosclerosis. World J Cardiol 2015;7:776–83. http://dx.doi.org/10.4330/wjc.v7.i11.776.
[17] Hoshino T, Chow LA, Hsu JJ, Perlowski AA, Abedin M, Tobis J, et al. Mechanical stress analysis of a rigid inclusion in distensible material: a model of atherosclerotic calcification and plaque vulnerability. Am J Physiol Heart Circ Physiol 2009;297:H802–10. http://dx.doi.org/10.1152/ajpheart.00318.2009.
[18] Kelly-Arnold A, Maldonado N, Laudier D, Aikawa E, Cardoso L, Weinbaum S. Revised microcalcification hypothesis for fibrous cap rupture in human coronary arteries. Proc Natl Acad Sci U S A 2013;110:10741–6. http://dx.doi.org/10.1073/pnas.1308814110.
[19] Akahori H, Tsujino T, Naito Y, Matsumoto M, Lee-Kawabata M, Ohyanagi M, et al. Intraleaflet haemorrhage is associated with rapid progression of degenerative aortic valve stenosis. Eur Heart J 2011;32:888–96. http://dx.doi.org/10.1093/eurheartj/ehq479.
[20] Virmani R, Kolodgie FD, Burke AP, Finn AV, Gold HK, Tulenko TN, et al. Atherosclerotic plaque progression and vulnerability to rupture: angiogenesis as a source of intraplaque hemorrhage. Arterioscler Thromb Vasc Biol 2005;25:2054–61. http://dx.doi.org/10.1161/01.ATV.0000178991.71605.18.
[21] Kolodgie FD, Burke AP, Nakazawa G, Cheng Q, Xu X, Virmani R. Free cholesterol in atherosclerotic plaques: where does it come from? Curr Opin Lipidol 2007;18:500–7. http://dx.doi.org/10.1097/MOL.0b013e3282efa35b.
[22] Arbustini E, Morbini P, D'Armini AM, Repetto A, Minzioni G, Piovella F, et al. Plaque composition in plexogenic and thromboembolic pulmonary hypertension: the critical role of thrombotic material in pultaceous core formation. Heart 2002;88:177–82. http://dx.doi.org/10.1136/heart.88.2.177.
[23] Roschzttardtz H, Conéjéro G, Curie C, Mari S. Straightforward histochemical staining of Fe by the adaptation of an old-school technique: identification of the endodermal vacuole as the site of Fe storage in *Arabidopsis* embryos. Plant Signal Behav 2010;5:56–7. http://dx.doi.org/10.1104/pp.109.144444.
[24] Nagy E, Eaton JW, Jeney V, Soares MP, Varga Z, Galajda Z, et al. Red cells, hemoglobin, heme, iron, and atherogenesis. Arterioscler Thromb Vasc Biol 2010;30:1347–53. http://dx.doi.org/10.1161/ATVBAHA.110.206433.
[25] Miller YI, Shaklai N. Oxidative crosslinking of LDL protein induced by hemin: involvement of tyrosines. Biochem Mol Biol Int 1994;34:1121–9.
[26] Balla G, Jacob HS, Eaton JW, Belcher JD, Vercellotti GM. Hemin: a possible physiological mediator of low density lipoprotein oxidation and endothelial injury. Arterioscler Thromb 1991;11:1700–11. http://dx.doi.org/10.1161/01.ATV.11.6.1700.
[27] Abraham NG, Lavrovsky Y, Schwartzman ML, Stoltz RA, Levere RD, Gerritsen ME, et al. Transfection of the human heme oxygenase gene into rabbit coronary microvessel endothelial cells: protective effect against heme and hemoglobin toxicity. Proc Natl Acad Sci U S A 1995;92:6798–802.
[28] Moreno PR, Purushothaman KR, Purushothaman M, Muntner P, Levy NS, Fuster V, et al. Haptoglobin genotype is a major determinant of the amount of iron in the human atherosclerotic plaque. J Am Coll Cardiol 2008;52:1049–51. http://dx.doi.org/10.1016/j.jacc.2008.06.029.
[29] Lin HL, Zhang L, Liu CX, Xu XS, Tang MX, Lv HX, et al. Haemin-enhanced expression of haem oxygenase-1 stabilizes erythrocyte-induced vulnerable atherosclerotic plaques. Br J Pharmacol 2010;160:1484–95. http://dx.doi.org/10.1111/j.1476-5381.2010.00799.
[30] Takano M, Yamamoto M, Inami S, Murakami D, Ohba T, Seino Y, et al. Appearance of lipid-laden intima and neovascularization after implantation of bare-metal stents extended late-phase observation by intracoronary optical coherence tomography. J Am Coll Cardiol 2009;55:26–32. http://dx.doi.org/10.1016/j.jacc.2009.08.032.
[31] Michel J-B, Thaunat O, Houard X, Meilhac O, Caligiuri G, Nicoletti A. Topological determinants and consequences of adventitial responses to arterial wall injury. Arterioscler Thromb Vasc Biol 2007;27:1259–68. http://dx.doi.org/10.1161/ATVBAHA.106.137851.
[32] Thaunat O, Patey N, Morelon E, Michel J-B, Nicoletti A. Lymphoid neogenesis in chronic rejection: the murderer is in the house. Curr Opin Immunol 2006;18:576–9. http://dx.doi.org/10.1016/j.coi.2006.07.006.
[33] Weih F, Gräbner R, Hu D, Beer M, Habenicht AJR. Control of dichotomic innate and adaptive immune responses by artery tertiary lymphoid organs in atherosclerosis. Front Physiol 2012;3:226. http://dx.doi.org/10.3389/fphys.2012.00226.
[34] Clement M, Guedj K, Andreata F, Morvan M, Bey L, Khallou-Laschet J, et al. Control of the T follicular helper-germinal center B-cell axis by $CD8^{+}$ regulatory T cells limits atherosclerosis and tertiary lymphoid organ development. Circulation 2015;131:560–70. http://dx.doi.org/10.1161/CIRCULATIONAHA.114.010988.
[35] Otsuka F, Nakano M, Ladich E, Kolodgie FD, Virmani R. Pathologic etiologies of late and very late stent thrombosis following first-generation drug-eluting stent placement. Thrombosis 2012;2012:608593. http://dx.doi.org/10.1155/2012/608593.
[36] Alfonso F, Fernandez-Viña F, Medina M, Hernandez R. Neoatherosclerosis: the missing link between very late stent thrombosis and very late in-stent restenosis. J Am Coll Cardiol 2013;61:e155. http://dx.doi.org/10.1016/j.jacc.2012.09.071.